Numerical Methods in Civil Engineering

Journal Homepage: https://nmce.kntu.ac.ir/

A modified scaled boundary method to analyze structural elements

Ali Zareh*, Ramin Vafaei Poursorkhabi *,**, Alireza Alizadeh Majdi *, and Fariba Behrouz Sarand*

Abstract:

It is possible to resolve numerical issues by utilizing a method known as the conventional scaled boundary finite element method (also known as SBFEM), which is a dimension reduction technique. This method can be utilized in conjunction with mesh-free technologies in order to enhance the numerical characteristics of the conventional SBFEM. Within the scope of this investigation, a novel interpretation of the SBM is presented that makes use of the advantages offered by the meshless local Petrov Galerkin method. Using the moving Kriging interpolation (MKI) method, it is possible to create shape functions that conform to the requirements of the Kronecker delta function property. The interpolating scaled boundary local Petrov Galerkin method that was then proposed has the ability to implement essential boundary conditions (ISBLPGM) directly. This new method offers a number of benefits in comparison to scaled boundary approaches that have been presented in the past. It is optional to have a mesh that has been predefined, and the boundary conditions can be determined with very little additional effort. It has been demonstrated that the numerical approach being presented yields results that are in very good agreement with analytical and other numerical approaches. Solving the benchmark numerical problems allows an evaluation of the effectiveness of the proposed method as well as its precision.

1. Introduction

Partial differential equations (PDEs) can be applied to the majority of engineering problems in order to define and solve them. These strong forms of equations are amenable to being solved numerically through using methods such as continuum and discrete mechanics-based methods [1]. Some numerical techniques, such as the finite difference method (FDM), are utilized to solve partial differential equations and previously used to approximate their solutions. The method of finite differences is a powerful numerical technology that has been utilized in the past for a variety of different types of analyses [2, 3].

In some circumstances, it may be possible to arrive at a more workable solution by lowering the order of the differential equations.

Utilizing the weighted residual method [4] is a way to order of differential equations can be reduced to integral equations. The resulting integral equations, sometimes referred to as weak-form equations, can be analyzed by applying a wide variety of numerical methods.

Regarding problems involving PDEs in their weak form, the traditional finite element method, also known as FEM, is useful for approximating solutions. For example, the finite element method can be utilized to investigate both elastostatics and elastodynamics successfully [5, 6].

However, the FEM and the FDM are useful tools for numerical computation, but both of these approaches also have some limitations in dealing with various mechanical problems. These conventional numerical methods are only capable of conducting an analysis of unbounded media by adding various numerical approximations and making assumptions. In both the FEM and the FDM, it is necessary to discretize the entire domain. The finite element model (FEM) needs to use predefined shape functions, and can increase the level of accuracy, particularly for stresses.

* Department of Civil Engineering, Tabriz Branch, Islamic Azad University, Tabriz, Iran.
** Corresponding author: Robotics & Soft Technologies Research Centre, Tabriz Branch, Islamic Azad University, Tabriz, Iran, raminvafaei@yahoo.com, vafaei@iaut.ac.ir

Mesh-free technologies have the potential to be viable alternatives for the solution of partial differential equations. The application of mesh-free methods can significantly reduce the drawbacks of FDM and FEM, that have been previously discussed. These methods eliminate the requirement for a unique mesh, and the resultant stress field has the potential to be more accurate than those produced by FDM and FEM, respectively. There have been many different mesh-free methodologies developed up until this point. As an illustration, the mesh-free (or meshless) local Petrov-Galerkin (MLPG) method [9], the element-free Galerkin (EFG) technology [7], the reproducing kernel particle approach (RKPM) [8], and the radial point interpolation method [10] were all developed.

For the purpose of resolving either the weak or the strong form of PDEs, discretizing boundary methods is an alternative to full-domain discretizing techniques (FEM and FDM). The boundary element method is a well-known numerical method that provides solutions to problems by discretizing domain boundaries (BEM). Recent engineering research has made use of the time-tested boundary element method (BEM) to investigate a wide range of engineering problems. The BEM was able to analyze seepage, as well as static [11, 12], dynamic [15, 16], and static [13, 14] issues successfully. For the boundary element method to work, the essential or fundamental solution, also known as the Green function, must satisfy the governing equations present in the problem's domain [17]. Calculating this analytical solution for a number of different problems could take a significant amount of time. The main disadvantage of the BEM is its reliance on a fundamental solution. SBM does not need any fundamental solution. In comparison with the PML, SBM is very similar in derivation and solving procedures. But the SBM can reduce the dimensional problem by one.

In the past twenty years, Wolf and Song [18] have proposed a procedure for boundary discretization. This procedure uses finite element technology to solve problems on the boundary of the domain, while an analytical approach is used to solve problems in the interior of the domain. The Scaled Boundary Method (SBM), which is a relatively new methodology, does not require any Green function (unlike the conventional BEM). This semi-analytical approach (the scaled boundary method) combines the benefits of two of the most popular FEM and BEM approaches. Within the SBM, the Cartesian coordinate system needs to be converted into an entirely new coordinate system (scaled boundary coordinate system). The achieved partial differential equations in the mapped system can be expressed in the new form using a scaling centre (SC) and two dimensionless local coordinates (η, ξ). It is possible for two-dimensional (2D) problems. The scaled boundary method's domain discretization scheme is illustrated in Figure 1.

Fig. 1: Domain discretization scheme of the scaled boundary method.

In the past, a number of different problems have been tackled with the assistance of the scaled boundary method. Seepage [20, 21], static [22, 23], and dynamic issues [24, 25] are all examples of problems that have been analysed using this method.

The traditional SBM can be modified in a variety of different ways to achieve better or similar results (in a more efficient manner) using this strategy. In recent decades, there has been an increased focus on the envisioned benefits resulting from the combination of" for clarity mesh-free technology with SBM [37]. Boundary discretization mesh-free methods are the only way to solve governing differential equations, and they achieve this only by discretizing the problem's boundary. This allows for a significant reduction in the number of degrees of freedom (DOFs) in the model. It is possible to consider the boundary node method (BNM), which was initially proposed by Mukherjee and Mukherjee in 1997 [26], as one of the pioneering boundary-type mesh-free methods that were suggested in this area of research. Zhu and Atluri [27] presented the LBIE method, which stands for the local boundary integral equation. Both the BNM and the LBIE construct shape functions along with their derivatives with the help of an approximation known as moving least squares (MLS). As a direct consequence of this, the Kronecker delta function property is not satisfied by the aforementioned procedures. For the purpose of analysing engineering problems, Liu and Gu [28] proposed the boundary point interpolation method, also known as BPIM. Because shape functions are built with the boundary point interpolation method, which employs the point interpolation technique, the Kronecker delta function property is possessed by shape functions.

Enhanced versions of the original SBM were presented in the past using the concept of meshless numerical algorithms. These enhanced versions were based on the local Petrov Galerkin and element-free Galerkin numerical technologies [29, 30]. These methodologies obtain their results by applying the MLS approximation to the data. Because the application of the MLS approximation in the construction of shape functions results in non-interpolating functions, these

studies present a brand-new method for modifying the MLS shape functions. The new procedure does provide the interpolating MLS shape functions; however, as a result of utilizing it, the scaled boundary mesh-free methods that were discussed earlier become excruciatingly sluggish and time-consuming.

Recently, a number of researchers have been successful in solving engineering problems by employing a technique known as the radial point interpolation-based scaled boundary method (RPISBM). Investigations into two-dimensional elasto-static problems [33], crack problems [32], and fracture analysis of piezoelectric material [31] were all conducted with the assistance of the RPISBM. Because the boundary of the 2D problems is one-dimensional, using a radial basis in the scaled boundary point interpolation technology is not required. However, the use of radial basis is still possible. Hasanzadeh et al. [34] proposed a PIM-based scaled boundary mesh-free method as a solution to seismic soil-structure interaction problems.

In the current investigation, a novel scaled boundary mesh-free method is presented. This method has been created by combining the standard SBM with the meshless local Petrov Galerkin method. In order to generate shape functions for the scaled boundary method, [35] we have made use of the moving Kriging interpolation (MKI) method for the very first time. The proposed interpolating scaled boundary local Petrov Galerkin method can easily incorporate necessary boundary conditions thanks to the Kronecker delta function property of the shape functions that are produced by the MKI (ISBLPGM). This new method offers a number of benefits in contrast to scaled boundary approaches that have been presented in the past. Both the definition of boundary conditions and the creation of a predefined mesh are optional, and the former does not require any additional labor. The following is an outline of the paper's structure: The fundamental equations of the interpolating scaled boundary local Petrov Galerkin method are broken down in excruciating detail in the following section of this article. In this section, a number of numerical examples that serve as benchmarks will be solved in order to assess the accuracy of the proposed methodology and to demonstrate how effective this novel numerical approach is. In the final section, we cover the discussions, and then we draw some conclusions.

2. The interpolating scaled boundary local Petrov Galerkin method

An analytical approach is taken in the radial direction, while a numerical approach is taken in the circumferential direction when the SBM is first proposed (as a boundary element method without the requirement of essential solutions or Green functions). Because of this, the SBM can

be viewed as a method semi-analytical [36]. A mapping strategy is utilized in the conventional SBM in order to convert the governing PDE to a set of ODEs (Cauchy–Euler differential equations in the case of static models). Within the context of the SBM, the domain edge is discretized in relation to a specific point (which should be visible from the whole of the boundary and can be named the scale centre). As has been previously stated, the point that is chosen to serve as the scale centre, which is denoted by the coordinates (x_0, y_0), must be visible from every single point on the boundary of the domain (as shown in Figure 1). The mapping procedure of the domain from the Cartesian coordinate system to the scaled boundary coordinate system is the primary example of the mathematical work required in the application of the SBM. Following this procedure for mapping, each point in the scaled boundary coordinate system can be defined by using the coordinates of the scale centre and the corresponding point in the discretized boundary, as shown by Equations (1) and (2):

$$x(\xi) = x_0 + \xi \, x(\eta) \tag{1}$$

$$y(\xi) = y_0 + \xi \, y(\eta) \tag{2}$$

In the equations that are presented, ξ and η stand for the radial coordinate and the circumferential coordinate, respectively. It is possible to extract the field variable by making use of the new coordinate system if such a geometrical mapping procedure is used, as it is defined in Equation (3).

$$\{u_h(\xi, \eta)\} = [N_h(\eta)]\{u_h(\xi)\} \tag{3}$$

$u_h(\xi)$ is a set of n functions of [30], and in this equation, $[N_h(\eta)]$ is the matrix of shape functions. Equation (4) can be used to determine the strains present in the scaled boundary coordinate system (4).

$$\{\varepsilon_h(\xi, \eta)\} = [L].\{u_h(\xi, \eta)\} \tag{4}$$

Because the boundary of the domain is mapped to the scaled boundary coordinate system, the conventional differential operator L cannot be used to calculate strains in the new system; rather, a new operator called L* must be used in its place. This is because the new system is a different kind of differential operator. The following is one way to define this brand-new operator:

$$[L^*] = [b^1(\eta)] \frac{\partial}{\partial \xi} + \frac{1}{\xi} [b^2(\eta)] \frac{\partial}{\partial \eta} \tag{5}$$

Where $[b^1(\eta)]$ and $[b^2(\eta)]$ represent the coordinate functions and the shape functions, respectively. These matrices can be calculated using Equation (6) and Equation (7).

$$[b^1] = \frac{1}{|jac|} \begin{bmatrix} y(\eta),\eta & 0 \\ 0 & -x(\eta),\eta \\ -x(\eta),\eta & y(\eta),\eta \end{bmatrix} \tag{6}$$

$$[b^2] = \frac{1}{|jac|} \begin{bmatrix} -y(\eta) & 0 \\ 0 & x(\eta) \\ x(\eta) & -y(\eta) \end{bmatrix} \tag{7}$$

In these equations, $|j_{ac}|$ represents the Jacobean of the support domain and its value can be calculated as follows:

$$|jac| = x(\eta)y(\eta)_{,\eta} - y(\eta)x(\eta)_{,\eta} \tag{8}$$

In Equation (8), local coordinates and derivatives of them can be calculated as follows:

$$x(\eta) = [N_1(\eta)N_2(\eta)N_3(\eta) \dots \dots N_N(\eta)] \begin{Bmatrix} x_1 \\ x_2 \\ \vdots \\ x_n \end{Bmatrix} \tag{9}$$

$$y(\eta) = [N_1(\eta)N_2(\eta)N_3(\eta) \dots \dots N_N(\eta)] \begin{Bmatrix} y_1 \\ y_2 \\ \vdots \\ y_n \end{Bmatrix} \tag{10}$$

$$x(\eta),\eta = [N_1(\eta)N_2(\eta)N_3(\eta) \dots \dots N_N(\eta)],\eta \begin{Bmatrix} x_1 \\ x_2 \\ \vdots \\ x_n \end{Bmatrix} \tag{11}$$

$$y(\eta),\eta = [N_1(\eta)N_2(\eta)N_3(\eta) \dots \dots N_N(\eta)],\eta \begin{Bmatrix} y_1 \\ y_2 \\ \vdots \\ y_n \end{Bmatrix} \tag{12}$$

It is possible to determine the strain field by combining Equation 3, 4, and 5, and then it is possible to determine the stress field by multiplying the resulting strain field by an elasticity matrix using the resultant strain field. The resulting stress field relationship for the scaled boundary method is displayed in Equation 13.

$$\begin{aligned} \{\sigma(\xi,\eta)\} &= [D]\{\varepsilon(\xi,\eta)\} \\ &= [D][B^{11}(\eta)]\{u_h(\xi)\}_{,\xi} \\ &\quad + \frac{1}{\xi}[D]\{\varepsilon(\xi,\eta)\} \\ &= [D][B^{21}(\eta)]\{u_h(\xi)\} \end{aligned} \tag{13}$$

Where

$$[B^{11}(\eta)] = [b^1(\eta)][N(\eta)] \tag{14}$$

$$[B^{21}(\eta)] = [b^{21}(\eta)][N(\eta)]_{,\eta} \tag{15}$$

In order to fulfil the equilibrium requirement, the term "virtual work" should be implemented. In the local Petrov Galerkin method, in contrast to the Galerkin-based methods, the virtual displacement field is formed by using the test functions *[w(η)]*, where the defined test functions are separate from the shape functions. In other words, the test functions are not the same thing as the shape functions. In light of the information presented above, the virtual displacement field can be stated as follows:

$$\{\delta u(\xi,\eta)\} = [w(\eta)]\{\delta u(\xi)\} \tag{16}$$

Using Equation 4 and Equation 5, the virtual strain field can be introduced like Equation 17.

$$\begin{aligned} \{\delta\varepsilon(\xi,\eta)\} &= [L^*]\{\delta u(\xi,\eta)\} = [L^*][w(\eta)]\{\delta u(\xi)\} \\ &= [B^{12}(\eta)]\{\delta u(\xi)\}_{,\xi} \\ &\quad + \frac{1}{\xi}[B^{22}(\eta)]\delta\{u_h(\xi)\} \end{aligned} \tag{17}$$

Where

$$[B^{12}(\eta)] = [b^1(\eta)][w(\eta)] \tag{18}$$

$$[B^{22}(\eta)] = [b^2(\eta)][w(\eta)]_{,\eta} \tag{19}$$

The principle of virtual work (by ignoring body force) can be written as:

$$\int_v \{\delta\varepsilon(\xi,\eta)\}^T \{\sigma_h(\xi,\eta)\}dV - \int_s \{\delta u(\eta)\}^T \{t(\eta)\}dS = 0 \tag{20}$$

Where the first and the second terms are related to the internal and the external work, respectively. By substituting Equation (17) and Equation (13) into the corresponding terms in Eq. (20) and after some mathematical manipulation, the expression of virtual work yields:

$$\begin{aligned} \{\delta u\}^T &([E^{11}]\{u\}_{,\xi} \\ &+ [E^{12}]^T\{u\}) \int_0^1 \{\delta u(\xi)\}^T [[E^{11}]\xi\{u_h(\xi)\}_{,\xi\xi} + [E^{11}] \\ &+ [E^{12}]^T - [E^{21}]]\left\{u(\xi)\right\}_{,\xi} - [E^{22}]\frac{1}{\xi}\{u(\xi)\}\right] d\xi \\ &- \{\delta u\}^T \int_{\eta=-1}^{\eta=+1} [w]^T \{t(\eta)\}d\eta = 0 \end{aligned} \tag{21}$$

In the above equation, E^{11}, E^{12}, E^{21}, and E^{22} are coefficient matrices of the scaled boundary local Petrov Galerkin method and can be defined as follows:

$$x(\eta) = [N_1(\eta)N_2(\eta)N_3(\eta) \dots \dots N_N(\eta)] \begin{Bmatrix} x_1 \\ x_2 \\ \vdots \\ x_n \end{Bmatrix} \tag{22}$$

$$y(\eta) = [N_1(\eta)N_2(\eta)N_3(\eta) \dots \dots N_N(\eta)] \begin{Bmatrix} y_1 \\ y_2 \\ \vdots \\ y_n \end{Bmatrix} \tag{23}$$

$$x(\eta),\eta = [N_1(\eta)N_2(\eta)N_3(\eta) \dots \dots N_N(\eta)],\eta \begin{Bmatrix} x_1 \\ x_2 \\ \vdots \\ x_n \end{Bmatrix} \tag{24}$$

$$y(\eta),\eta = [N_1(\eta)N_2(\eta)N_3(\eta) \dots \dots N_N(\eta)],\eta \begin{Bmatrix} y_1 \\ y_2 \\ \vdots \\ y_n \end{Bmatrix} \tag{25}$$

In the above equations, $[D]$ is the elasticity matrix. It should be noted that $|J|$ in Equations (22-25) is not identical to $|jac|$ in Equations (6-7). $|j_{ac}|$ is the Jacobean of the support domain, while $|J|$ is the Jacobean of the integration cell. By setting both terms of Eq. (21) to zero, Equation (26) and

Equation (27) can be achieved. The solution procedure of these equations is explained in detail in [29].

$$\{P\} = [E^{11}]\{u\}_{,\xi} + [E^{12}]\{u\} \tag{26}$$

$$[E^{11}]\xi^2\{u(\xi)\}_{,\xi\xi} + \big[[E^{11}] + [E^{12}] - [E^{21}]\big]\xi\{u(\xi)\}_{,\xi} \\ - [E^{22}]\{u(\xi)\} = \{0\} \tag{27}$$

In the current work, the moving Kriging interpolation (MKI) method is used to create the shape functions and their derivatives. The MKI shape functions can be determined using Equation (28).

$$\{N(\eta)\} = \{p(\eta)\}^T[A] + \{r(\eta)\}^T[B] \tag{28}$$

Where $\{p(\eta)\}$ is the vector of polynomial basis (for the related Gauss point). Other coefficient matrices can be determined by:

$$[A] = ([P]^T[R]^{-1}[P])^{-1}[P]^T[R]^{-1} \tag{29}$$

$$[B] = [R]^{-1}([I] - [P][A]) \tag{30}$$

$$\{r(\eta)\}^T = \{\gamma(\eta,\eta_1) \dots \gamma(\eta,\eta_N)\} \tag{31}$$

Observe that in the above equations N is the number of nodes in the support domain, and [I] is the unit matrix. The matrices of [P] and [R] should be calculated by:

$$[P] = \begin{bmatrix} 1 & \eta_1 & \eta_1{}^2 & \dots & \eta_1{}^{m-1} \\ 1 & \eta_2 & \eta_2{}^2 & \dots & \eta_2{}^{m-1} \\ 1 & \eta_3 & \eta_3{}^2 & \dots & \eta_3{}^{m-1} \\ \vdots & \vdots & \vdots & \ddots & \vdots \\ 1 & \eta_N & \eta_N{}^2 & \dots & \eta_N{}^{m-1} \end{bmatrix} \tag{32}$$

$$[P]$$
$$= \begin{bmatrix} \gamma(\eta_1,\eta_1) & \gamma(\eta_1,\eta_2) & \gamma(\eta_1,\eta_3) & \dots & \gamma(\eta_1,\eta_N) \\ \gamma(\eta_2,\eta_1) & \gamma(\eta_2,\eta_2) & \gamma(\eta_2,\eta_3) & \dots & \gamma(\eta_2,\eta_N) \\ \gamma(\eta_3,\eta_1) & \gamma(\eta_3,\eta_2) & \gamma(\eta_3,\eta_3) & \dots & \gamma(\eta_3,\eta_N) \\ \vdots & \vdots & \vdots & \ddots & \vdots \\ \gamma(\eta_N,\eta_1) & \gamma(\eta_N,\eta_2) & \gamma(\eta_N,\eta_3) & \dots & \gamma(\eta_N,\eta_N) \end{bmatrix} \tag{33}$$

In Equation (33), the variable γ can be defined using the following:

$$\gamma(\eta_i,\eta_j) = e^{-c\|\eta_i - \eta_j\|^2} \tag{34}$$

Where c is a constant number smaller than one. The constructed shape functions using Equation (28) has the property of the Kronecker delta function. The first-order derivation of the shape functions can be determined straightforwardly by:

$$\{N(\eta)\}_{,\eta} = \{p(\eta)\}_{,\eta}{}^T[A] + \{r(\eta)\}_{,\eta}{}^T[B] \tag{35}$$

For simplicity, the used test functions are selected equal to the $\{r(\eta)\}$ in Equation (31).

3. Numerical verifications

In this section, three benchmark numerical examples are solved by the proposed ISBLPG method to evaluate the accuracy and efficiency of this approach.

3.1 Cantilever beam subjected to a uniformly distributed load

As the first example, a cantilever beam which is subjected to a uniformly distributed load at the end of the beam, is selected to analyze. Material properties are as follows E=100000 kPa (elastic modulus), v=0.33 (Poisson's ratio). The geometrical dimensions of the beam being considered are selected as L=12, D=8. The prescribed model for this investigation is shown in Fig. 2. The load intensity is chosen as 2.5 KN.

The exact solution to this problem was presented in the literature. Displacement in the y-direction can be determined using:

$$u_y(x, y = 0) = \frac{p}{6EI}\left((4 + 5v)\frac{D^2 x}{4} + (3L - x)x^2\right) \tag{36}$$

Where I is the moment of inertia. Figure 3.a illustrates the deformed shape of the beam, and Figure 3.b depicts the displacements calculated along the length of the beam.
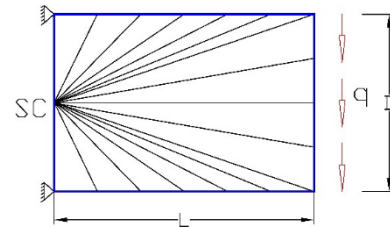

Fig. 2: Prescribed cantilever beam model and applied load for the first example.

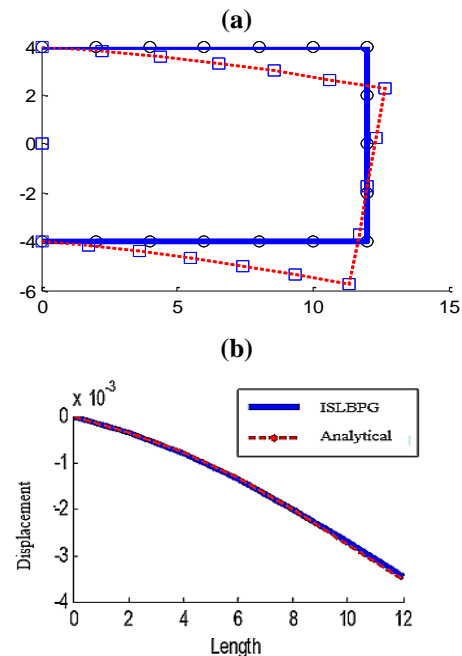As can be seen from this figure, excellent agreement is achieved between the ISBLPGM and the exact solution.

Fig. 3: (a) Deformed shape of the beam (500 times larger than the real answer). (b) The calculated and the exact displacements along the length of the beam.

3.2 Cantilever beam subjected to a bending moment

For the second example, another cantilever beam which is subjected to a bending moment at the end of the beam, has been. Material properties are as follows E=1000 kPa (elastic modulus), v=0 (Poisson's ratio). The geometrical dimensions of the beam being considered are selected as L=12, D=8. The prescribed model for this investigation is shown in Figure 4. The magnitude of the bending moment is equal to 1kN.m.

The exact solution to this problem couldbe calculated using the principles of solid mechanics. Displacement in the y-direction can be determined using:

$$u(x) = \frac{Mx^2}{2EI} \tag{37}$$
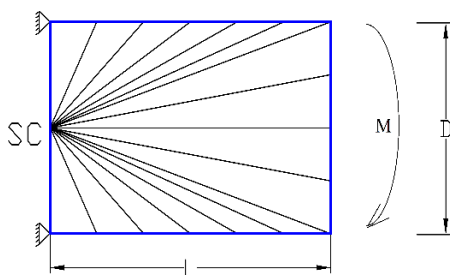
Fig. 4: Prescribed cantilever beam model and applied bending moment for the second example.

Where I is the moment of inertia. Figure 5.a depicts the deformed shape of the beam, and Figure 5.b illustrates the calculated displacements occurring along the length of the beam. According to what is displayed in this figure, the ISBLPGM and the analytical solution achieve a very high level of agreement.
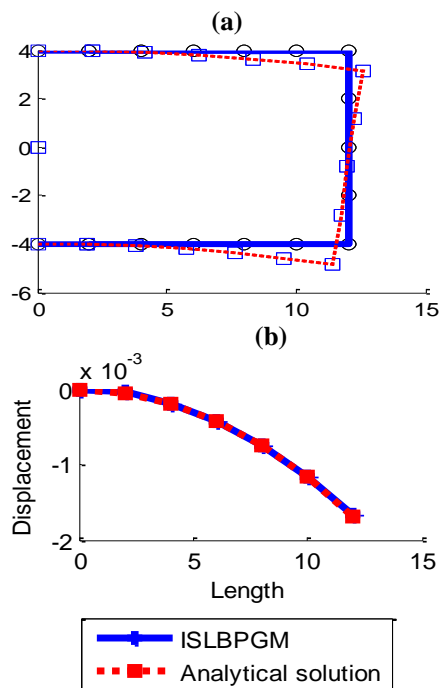
Fig. 5: (a) Deformed shape of the beam under bending moment (500 times larger than the real answer). (b) The calculated and the analytical solution of displacements along the length of the beam.

3.3 Cook membrane problem

For the last example, cook membrane problem is selected to solve. Cook membrane is a clamped cantilever beam, which is subjected to a uniformly distributed load at the end of the beam. Material properties are as follows E=1 (elastic modulus), v=1/3 (Poisson's ratio). The geometrical dimensions of the beam being considered are detailed in Figure 6. The magnitude of the concentrated load is 1, is applied at the end of the beam with a uniform distribution.
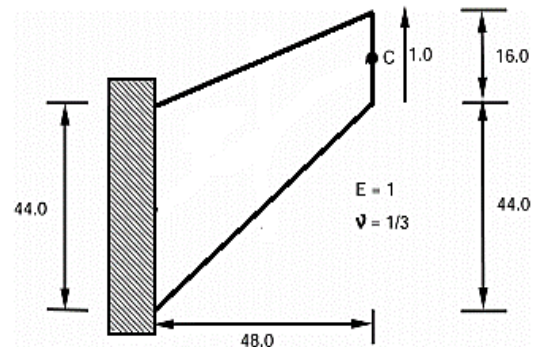
Fig. 6: Geometrical dimensions of the Cook membrane problem.

The exact solution to this problem could be obtained from the literature. In this analysis, displacement of Point C is calculated using the finite element method and the interpolating scaled boundary local Petrov Galerkin methods. Different numbers of nodes are used to evaluate the convergence path of the mentioned methods. Figure 7 shows the deformed shape of the Cook membrane for one of the selected nodes.
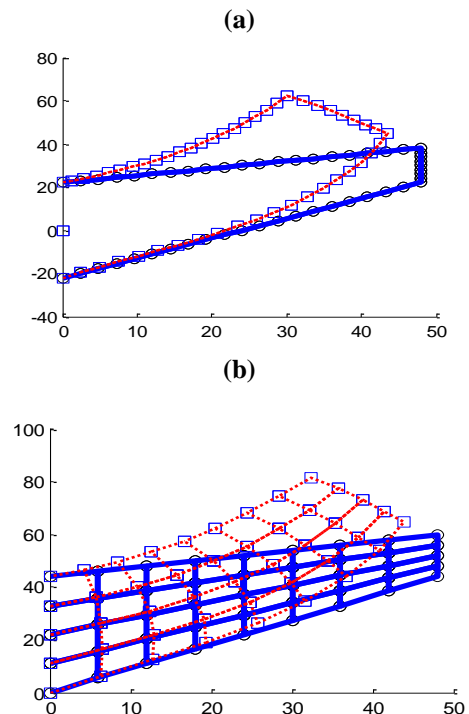

Fig. 7: Deformed shape of the Cook membrane in the a) FEM and b) ISBLPGM.

Convergence paths of the FEM and the ISBLPGM have been shown in Figure 8. As this figure shows, the proposed

scaled boundary meshless method can rapidly lead to the exact solution with a few numbers of nodes. In the case of the FEM, it is obvious that this method needs a large number of nodes in comparison with the ISBLPGM.
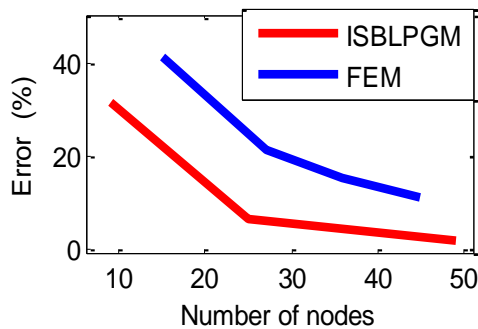

Fig. 8: Convergence paths of the FEM and the ISBLPGM.

The BEM (a well-known boundary discretizing method) has previously been mostly used for unbounded domain problems. Therefore, a comparison between the results of the proposed method with the BEM is impossible for the authors. However, as the BEM could be considered a semi-analytical method, the previously published studies show the same level of accuracy between SBM and BEM. For example, Hassanzadeh et al. [34] compared the results of a mesh-free SBM with BEM and demonstrated that both methods lead to the same accuracy.

4. Conclusion

An interpolating mesh-free scaled boundary local Petrov Galperin method was presented in this paper as a means of analysing elastostatics problems. As is the case with other scaled boundary methods, the proposed ISBLPGM does not require a fundamental solution. Three benchmark numerical examples were used to illustrate how this mesh-free scaled boundary approach can be applied in practice. The results of the proposed model and the analytical solutions were able to agree with one another in a very satisfying manner. It is shown that the error of the proposed method could lead to 1% by a mesh refining procedure, while the error of the FEM could only decrease to 10% by the same refinement. It is revealed by the solved examples that the proposed SBM has no more than a 1% error in comparison with the analytical results. In addition, it has been demonstrated that the ISBLPGM has a better convergence (to the exact solution) when contrasted with the conventional finite element method. Therefore, it is possible to draw the conclusion that the proposed boundary-type mesh-free method is capable of accurately modelling elastostatics problems.

References

[1] Liu, G. R. (2002). *Mesh-free methods, moving beyond the finite element method*. CRC press

[2] Vafaei Pousorkhabi, R. (2020). Investigating the Effect of Flow and Sediment Particles Characteristics on Sandy Sediments Transport in Circular Sections using Data Driven Methods. *Water and Soil Science*, 30(4), 75-87. doi: 10.22034/ws.2020.11649

[3] Hajialilue-Bonab, M., & Razavi, S. K. (2015). A study of soil-nailed wall behavior at limit states. *Proceedings of the Institution of Civil Engineers-Ground Improvement*, 169(1), 64-76. https://doi.org/10.1680/jgrim.14.00021

[4] Khalili-Maleki, M., Vafaei Pousorkhabi, R., Nadiri, A.A., & Dabiri, R. (2022). Prediction of hydraulic conductivity based on the soil grain size using supervised committee machine artificial intelligence. *Earth Science Informatics,* 15, 2571–2583. https://doi.org/10.1007/s12145-022-00848-x

[5] Zienkiewicz, O. C., Owen, D. R. J., & Lee, K. N. (1974) Least square-finite element for elasto-static problems. Use of 'reduced integration. *International Journal for Numerical Methods in Engineering*, 8(2), 341-358. https://doi.org/10.1002/nme.1620080212

[6] Farajniya, R., Poursorkhabi, R. V., Zarean, A., & Dabiri, R. (2022). Investigation of the arching in rock-fill dam ten years after the end of construction using Numerical analysis and monitoring. *Ferdowsi Civil Engineering*, 35(1), 59-74. https://doi.org/ 10.22067/JFCEI.2022.73934.1098

[7] Belytschko, T., Lu, Y. Y., Gu, L. (1994) Element-free Galerkin methods. *International Journal for Numerical Methods in Engineering*, 37(2), 229-256. https://doi.org/10.1002/nme.1620370205

[8] Liu, W. K., Jun, S., & Zhang, Y. F. (1995). Reproducing kernel particle methods. *International Journal for Numerical Methods in Fluids*, 20(8-9), 1081-1106. https://doi.org/10.1002/fld.1650200824

[9] Atluri, S. N., & Zhu, T. (1998). A new meshless local Petrov-Galerkin (MLPG) approach in computational mechanics. *Computational Mechanics*, 22(2), 117-127. https://doi.org/10.1007/s004660050346

[10] Liu, G. R., Zhang, G. Y., Gu, Y., & Wang, Y. Y. (2005). A mesh-free radial point interpolation method (RPIM) for three-dimensional solids. *Computational Mechanics*, 36(6), 421-430. https://doi.org/10.1007/s00466-005-0657-6

[11] Rafiezadeh, K., Ataie-Ashtiani, B. (2014). Transient free-surface seepage in three-dimensional general anisotropic media by BEM, *Engineering Analysis with Boundary Elements*, 46, 51-66. https://doi.org/10.1016/j.enganabound.2014.04.025

[12] Rafiezadeh, K., Ataie-Ashtiani, B. (2016) Three-dimensional flow in anisotropic zoned porous media using boundary element method, *Engineering Analysis with Boundary Elements*, 36, 812–824. https://doi.org/10.1016/j.enganabound.2011.12.002

[13] Mendonça, A. V., De Paiva, J. B. (2000). A boundary element method for the static analysis of raft foundations on

piles. *Engineering Analysis with Boundary Elements*, 24(3), 237-247. https://doi.org/10.1016/S0955-7997(00)00002-3

[14] Tanaka, M., Bercin, A. N. (1998). Static bending analysis of stiffened plates using the boundary element method. *Engineering Analysis with Boundary Elements*, 21(2), 147-154. https://doi.org/10.1016/s0955-7997(98)00002-2

[15] Li, Z. H., Ribe, N. M. (2012). Dynamics of free subduction from 3-D boundary element modeling. *Journal of Geophysical Research: Solid Earth,* 117(B6). https://doi.org/10.1029/2012JB009165

[16] Brebbia, C. A., Nardini, D. (1983). Dynamic analysis in solid mechanics by an alternative boundary element procedure. *Soil Dynamics and Earthquake Engineering*, 2(4), 228-233. https://doi.org/10.1016/S0955-7997(00)00031-X

[17] Brebbia, C. A., Telles, J. C. F., Wrobel, L. C. (2012). *Boundary element techniques: theory and applications in engineering*. Springer Science & Business Media. https://doi.org/10.1115/1.3169016

[18] Song, C., Wolf, J. P. (1997). The scaled boundary finite-element method—alias consistent infinitesimal finite-element cell method for elastodynamics. *Computer Methods in Applied Mechanics and Engineering*, 147(3-4), 329-355. https://doi.org/10.1016/S0045-7825(97)00021-2

[19] Deeks, A. J., Wolf, J. P. (2002). A virtual work derivation of the scaled boundary finite-element method for elastostatics. *Computational Mechanics*, 28(6), 489-504. https://doi.org/10.1007/s00466-002-0314-2

[20] Bazyar, M. H., Talebi, A. (2015). Transient seepage analysis in zoned anisotropic soils based on the scaled boundary finite-element method. *International Journal for Numerical and Analytical Methods in Geomechanics*, 39(1), 1-22. https://doi.org/10.1002/nag.2291

[21] Fengzhi, L. I. (2009). Scaled boundary finite-element method for seepage-free surfaces analysis. *Chinese Journal of Computational Physics*, 5, 004.

[22] Song, C., Wolf, J. P. (2000). The scaled boundary finite-element method–a primer: solution procedures. *Computers & Structures, 78(1-3), 211-225.* https://doi.org/10.1016/S0045-7949(00)00100-0

[23] Song, C., Wolf, J. P. (1999). Body loads in scaled boundary finite-element method. *Computer Methods in Applied Mechanics and Engineering*., 180(1-2), 117-135. https://doi.org/10.1016/S0045-7825(99)00052-3

[24] Tohidvand, H. R., Hajialilue-Bonab, M. (2014). Seismic soil-structure interaction analysis using an effective scaled boundary spectral element approach, *Asian Journal of Civil Engineering*, 15, 501-516.

[25] Hajialilue-Bonab, M., Tohidvand, H. R. (2015). A modified scaled boundary approach in the frequency domain with diagonal coefficient matrices. *Engineering Analysis with*

Boundary Elements, 50, 8-18. https://doi.org/10.1016/j.enganabound.2014.07.001

[26] Mukherjee, Y. X., Mukherjee, S., (1997). Boundary node method for potential problems, *International Journal for Numerical Methods in Engineering*, 40, 797-815. https://doi.org/10.1002/(SICI)1097-0207

[27] Zhu, T. & Atluri, S., N. (1998). A modified collocation and a penalty formulation for enforcing the essential boundary conditions in the element-free Galerkin method, *Computational Mechanics*, 21: 211-222. https://doi.org/10.1007/s004660050296

[28] Liu, G. R., Gu, Y., T. (2000) Coupling of element free Galerkin and hybrid boundary element methods using modified variational formulation, *Computational Mechanics*, 26(2): 166-173. https://doi.org/10.1007/s004660000164

[29] Deeks, A. J., Augarde, C. E. (2005). A meshless local Petrov–Galerkin scaled boundary method, *Computational Mechanics*, 36, 159–170. https://doi.org/10.1007/s00466-004-0649-y

[30] He, Y., Yang, H., Deeks, A. J. (2012). An Element free Galerkin (EFG) scaled boundary method, *Finite Elements in Analysis and Design,* 62, 28-35. https://doi.org/10.1016/j.finel.2012.07.001

[31] Chen, S. S., Wang, J., Li, Q. H. (2016). Two-dimensional fracture analysis of piezoelectric material based on the scaled boundary node method, *Chinese Physics*, 25(4): 1-8. https://doi.org/10.1088/1674-1056/25/4/040203

[32] Chen, S. S., Li, Q. H., Liu, Y. H. (2012) Scaled boundary node method applied to two-dimensional crack problems, *Chinese Physics*, 21(11): 1-9. https://doi.org/10.1088/1674-1056/21/11/110207

[33] Hajiazizi, M., & Graili, A. (2017). A scaled boundary radial point interpolation method for 2-D elasticity problems. *International Journal for Numerical Methods in Engineering*, 112(7), 832-851. https://doi.org/10.1002/nme.5534

[34] Hassanzadeh, M., Tohidvand, H.R., Hajialilue-Bonab, M., Javadi, A.A. (2018). Scaled boundary point interpolation method for seismic soil-tunnel interaction analysis, *Computers and Geotechnics*, 101, 208-216. https://doi.org/10.1016/j.compgeo.2018.05.007

[35] Gu, L. (2003). Moving kriging interpolation and element-free Galerkin method. *International Journal for Numerical Methods in Engineering*, 56(1), 1-11. https://doi.org/10.1002/nme.553

[36] Wolf, J.P., Song, C. (1996). *Finite-element modeling of unbounded media*, Chichester. Wiley.

[37] Zang, Q., Bordas, S. P., Liu, J., & Natarajan, S. (2023). NURBS-Enhanced polygonal scaled boundary finite element method for heat diffusion in anisotropic media with internal

heat sources. *Engineering Analysis with Boundary Elements*, 148, 279-292.